Available online at www.sciencedirect.com

ScienceDirect

journal homepage: www.elsevier.com/locate/he

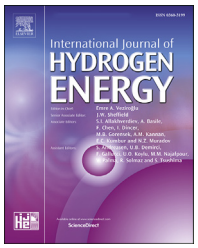

Local entropy generation and entropy fluxes of a transient flame during head-on quenching towards solid and hydrogen-permeable porous walls

Prashant S. Salimath, Ivar S. Ertesvåg *

Department of Energy and Process Engineering, Norwegian University of Science and Technology, Kolbjørn Hejes Vei 1b, NO-7491, Trondheim, Norway

HIGHLIGHTS

- Premixed hydrogen-air flame propagating towards a hydrogen-permeating wall.
- Entropy generation due to conductivity, mass diffusion and chemical reactions.
- Effects of initial temperature, fuel-air ratio and dilution.
- Entropy generation per unit of fuel reduced by fuel permeation into lean flame.

ARTICLE INFO

Article history:
Received 10 July 2020
Received in revised form
5 February 2021
Accepted 20 May 2021
Available online 18 June 2021

Keywords:
Entropy production
Entropy flux
Transient
Head-on quenching
Components of entropy generation
Detailed chemical mechanism

ABSTRACT

Premixed H_2-air flames are studied in a one-dimensional wall-bounded configuration. The laminar flame propagates towards and quenches at a wall that is either solid or permeable. Entropy generation by each of 19 elementary reactions is evaluated. Their total contribution remains the most important up to the quenching instance. Close to quenching, the conduction entropy generation grows considerable. Mass diffusion has a modest contribution, which decreases towards quenching. Viscous forces are negligible as a source of entropy. Effects of unburnt-mixture temperature and fuel-air ratio are investigated, and also dilution with nitrogen (inert) and water vapour. The diffusive entropy flux changed direction away from the permeating wall compared that of the solid wall. A major finding is that fuel permeation through the wall tends to decrease the entropy generation per unit of converted fuel, in particular for initially lean mixtures.

Introduction

Strive for less-polluting, more efficient and more compact combustion devices has led to more intensive combustion close to solid walls. These efforts also include new solutions like membrane reactors, where fuel or oxidizer are partly supplied through a porous wall into the combustor. Large efficiency losses can be the result of the concentrated fuel conversion close to solid surfaces. Some aspects of

* *Corresponding author.*
E-mail addresses: Prashant.Salimath@ntnu.no (P.S. Salimath), Ivar.S.Ertesvag@ntnu.no (I.S. Ertesvåg).
https://doi.org/10.1016/j.ijhydene.2021.05.142

flame-wall interactions were investigated by direct numerical computations in our previous studies [1–3], in which also the state of the art of head-on quenching was reviewed.

Efficiency of energy conversion is determined by the first and, in particular, the second law of thermodynamics. Degrading of energy is expressed in form of exergy destruction, aka. irreversibility, and entropy generation. In classical engineering thermodynamics, 2nd law analysis has come into use for industrial process simulations in the form of exergy analysis [4,5]. This method is used to evaluate and optimize thermal plants (e.g. Refs. [6,7]). Since spatial (and to a large extent temporal) gradients are neglected, it is sometimes called a "zero-dimensional" method.

Computational fluid dynamics (CFD) provides detailed knowledge of the fields of temperature, species concentration, heat and mass fluxes. Then, the entropy generation can be provided with a similar level of detail in space and time. The recent decades have seen increasing efforts in such approaches. Som and Datta [8] reviewed the state of the art up to 2006 for reacting flows. Arpaci and Selamet [9] were in 1988 "probably the first one" (in the wording of [8]) to apply this approach in combustion; for a flat premixed flame. Later, simulations have been conducted for laminar and turbulent flames in a variety of premixed and non-premixed configurations. The laminar, premixed flames were in the form of a 1-dimensional planar flame [10–13], a counterflow jet flame [14], axisymmetric annular combustors [15,16], a cylindrical recuperated micro combustor [17], microchannel and [18–20], micro-planar combustors [21]. In spite of the variations in set-up and geometries, these studies all found chemical reactions to give the largest contribution to entropy generation, followed by heat conduction and mass diffusion. For the case of transition from a planar propagating flame front to auto-ignition, Liu et al. [13] found that the chemical contribution became dominant at autoignition and that the heat and mass transfer vanished as sources of entropy. Laminar, non-premixed flames have been investigated by several authors, both single-phase flames and gaseous flames around a fuel droplet. Datta [22] (confined jet flame), Stanciu et al. [23] (jet flame), Nishida et al. [10] (jet flame), Datta [24] (confined jet flame with gravity), Chen et al. [25] (counterflow jet flame) and Briones et al. [26] (lifted jet flame, that is, partially premixed) all found heat conduction as the most important for entropy generation, followed by reactions and then mass diffusion. On the other hand, Chen et al. [27], found the chemical reactions to be more important for entropy generation along the axis of an opposing jet flame. Raghavan et al. [28] and Pope et al. [29] found heat conduction to be the largest contributor to entropy generation in the flame around a fuel droplet, closely followed by chemical reactions, while mass diffusion was less important. All the studies, both premixed and non-premixed, agreed that the contribution of viscous dissipation was negligible in premixed and non-premixed flames, except in zones where the other contributions were very small [25].

Turbulent reacting flows can be investigated by direct numerical simulation (DNS) similar to laminar flames. This has been done for very simple flames, but usually either chemistry or turbulence, or both, have to be dealt with by some sort of modeling and simplification. DNS with a single-step Arrhenius chemical model was used [30] to investigate entropy generation of a premixed flame in decaying turbulence at low Reynolds number. Other investigations were based on Reynolds-averaged Navier-Stokes (RANS) [23,31–34]. The modeling challenges faced by this approach were out of scope for the present study.

The majority of entropy-generation studies are made with the motivation of improving energy conversion. However, studies with other aims can also be found: Acoustic disturbances (noise) are related to entropy waves and generation of these. Investigations focused on thermal sources for such waves [35] and recently, also on differences in composition [36]. Furthermore, entropy has been related to soot formation [37], and used as a tool for reducing chemical mechanisms [38–40]. Another motivation has been to provide guidance with respect to realizability of physical submodels [41,42].

The present study was based on direct numerical computations [2] of a transient premixed laminar planar hydrogen flame propagating towards a solid wall, eventually quenching. Hydrogen permeation through the wall influences the overall head-on quenching (HOQ) process, including entropy generation and its components. Entropy generation through quenching has gained little attention in literature, and to our knowledge, entropy generation in HOQ flames has not been investigated previously.

The HOQ process involves flame propagation with reactions and heat losses. Large heat losses occur when the flame approaches the wall, which adversely affects hardware components and system performance. Conventional HOQ studies were performed for IW to understand near-wall reactions, heat transfer and flow physics. There is less focus towards understanding of irreversibilities during the HOQ process. In the present study, entropy analysis is performed for H_2 permeation on HOQ for different conditions and compared against convectional impervious wall boundary results, to understand processes and also assist in design to improve performance of system such as micro combustion.

In the following, the theoretical background is given in Section Models and numerical setup, with mathematical formulation of the entropy generation and entropy transport. In Section Results and discussion, first results for the free propagating premixed flame will be shown and compared with other investigations. Next, results for the head-on quenching towards the wall will be shown. Here, both the impermeable and the hydrogen-permeable cases are studied for an initially stoichiometric mixture. Subsequently, the effect lean and rich mixtures, the unburnt-mixture temperature and dilution will be shown and discussed. Finally, conclusions are made.

Models and numerical setup

Governing equations, properties and constitutive relations

The governing equations and relations are described according to Chen et al. [43], which documents the code used.

Momentum balance:

$$\frac{\partial}{\partial t}(\rho u_\alpha)+\frac{\partial}{\partial x_\beta}(\rho u_\alpha u_\beta)=-\frac{\partial p}{\partial x_\alpha}+\frac{\partial}{\partial x_\beta}(\tau_{\beta\alpha}) \tag{1}$$

Energy is expressed in form of the total specific internal energy with the balance equation,

$$\frac{\partial}{\partial t}(\rho e_0)+\frac{\partial}{\partial x_\beta}((\rho e_0+p)u_\beta)=-\frac{\partial q_\beta}{\partial x_\beta}+\frac{\partial}{\partial x_\beta}(\tau_{\beta\alpha}u_\alpha). \tag{2}$$

Species mass:

$$\frac{\partial}{\partial t}(\rho Y_i)+\frac{\partial}{\partial x_\beta}(\rho Y_i u_\beta)=\frac{\partial}{\partial x_\beta}(-J_{\beta i})+W_i\dot{\omega}_i. \tag{3}$$

The viscous stress, species diffusion velocity and heat flux are expressed as

$$\tau_{\alpha\beta}=\mu\left(\frac{\partial u_\beta}{\partial x_\alpha}+\frac{\partial u_\alpha}{\partial x_\beta}\right)-\frac{2}{3}\mu\frac{\partial u_\gamma}{\partial x_\gamma}\delta_{\alpha\beta}, \tag{4}$$

$$V_{\alpha i}=-\frac{D_i^{mix}}{X_i}d_{\alpha i}-\frac{D_i^T}{\rho Y_i}\frac{\partial}{\partial x_\alpha}(\ln T), \tag{5}$$

$$q_\alpha=-\lambda\frac{\partial T}{\partial x_\alpha}+\sum_{i=1}^{N_S}h_iJ_{\alpha i}-\sum_{i=1}^{N_S}\frac{p}{\rho Y_i}D_i^Td_{\alpha i}, \tag{6}$$

$$d_{\alpha i}=\frac{\partial X_i}{\partial x_\alpha}+(X_i-Y_i)\frac{\partial}{\partial x_\alpha}(\ln p) \tag{7}$$

The species mass flux can be split into three components; the species gradient diffusion flux (Fick), the pressure diffusion flux and the thermodiffusion (Soret) flux:

$$J_{\alpha i}=\rho Y_iV_{\alpha i}=J_{\alpha i}^{Fi}+J_{\alpha i}^{pd}+J_{\alpha i}^{So} \tag{8}$$

The heat flux of Eq. (6) has three components, viz. the conductive flux (Fourier), the heat flux due to species mass fluxes $J_{\alpha i}$ (which has three components, according to Eq. (8)), and the Dufour flux:

$$q_\alpha=q_\alpha^{Fo}+q_\alpha^J+q_\alpha^{Du} \tag{9}$$

It can be noted that in Eqs. (1) and (7), effects of body forces (gravity, electrochemical) are left out. Moreover, the bulk viscosity is set to zero in Eq. (4). The Dufour effect (last term of Eq. (6)) was not implemented in the code, however included here for reference.

A kinetic energy equation can be deduced from the momentum equation. Using the relation

$$e_0=h-\frac{p}{\rho}+\frac{1}{2}u_\alpha u_\alpha=e+\frac{1}{2}u_\alpha u_\alpha, \tag{10}$$

the energy equation, Eq. (2), can be reformulated to

$$\frac{\partial}{\partial t}(\rho e)+\frac{\partial}{\partial x_\beta}(\rho e u_\beta)=-\frac{\partial q_\beta}{\partial x_\beta}-p\frac{\partial u_\alpha}{\partial x_\alpha}+\tau_{\beta\alpha}\frac{\partial u_\alpha}{\partial x_\alpha} \tag{11}$$

The molar reaction rate of species i in Eq. (3) can be expressed from

$$\dot{\omega}_i=\sum_{j=1}^{N_R}\nu_{ij}q_j. \tag{12}$$

Here, $\nu_{ij}=\nu_{ij}''-\nu_{ij}'$ are the stoichiometric coefficients of reaction j, and

$$q_j=k_{fj}\prod_{i=1}^{N_S}\left(\frac{\rho Y_i}{W_i}\right)^{\nu_{ij}'}-k_{rj}\prod_{i=1}^{N_S}\left(\frac{\rho Y_i}{W_i}\right)^{\nu_{ij}''} \tag{13}$$

is the reaction progress. The forward rate coefficient is expressed as $k_{fj}=A_jT^{\beta_j}\exp(-E_j/(R_uT))$, while the reverse rate coefficient is expressed from the corresponding equilibrium constant, $k_{rj}=k_{fj}/K_{cj}$.

Entropy transport and generation

The numerical analysis of combustion is based on the equations above. By using the Gibbs relation for reacting systems, the entropy transport equation can be developed [44,45] as

$$\frac{\partial}{\partial t}(\rho s)+\frac{\partial}{\partial x_\beta}(\rho s u_\beta)=B_s+\sigma, \tag{14}$$

where the entropy diffusion term is

$$B_s=\frac{\partial}{\partial x_\beta}\left(\frac{1}{T}(-q_\beta^{Fo}-q_\beta^{Du})-\sum_{i=1}^{N_S}s_iJ_{\beta i}\right), \tag{15}$$

and the entropy generation rate is elaborated as the sum of contributions due to, respectively, viscous forces, conduction, Dufour flux, mass diffusion and chemical reactions:

$$\sigma=\sigma_{visc}+\sigma_{cond}+\sigma_{Du}+\sigma_{diff}+\sigma_{chem} \tag{16}$$

with

$$\sigma_{visc}=\frac{\tau_{\beta\alpha}}{T}\frac{\partial u_\alpha}{\partial x_\beta}, \tag{17}$$

$$\sigma_{cond}=\frac{1}{T^2}(-q_\beta^{Fo})\frac{\partial T}{\partial x_\beta}=\frac{\lambda}{T^2}\left(\frac{\partial T}{\partial x_\beta}\right)^2, \tag{18}$$

$$\sigma_{Du}=\frac{1}{T^2}(-q_\beta^{Du})\frac{\partial T}{\partial x_\beta}, \tag{19}$$

$$\sigma_{diff}=\sum_{i=1}^{N_S}(-J_{\beta i})\left(\frac{1}{T}\frac{\partial h_i}{\partial x_\beta}-\frac{\partial s_i}{\partial x_\beta}\right), \tag{20}$$

$$\sigma_{chem}=-\frac{1}{T}\sum_{i=1}^{N_S}g_iW_i\dot{\omega}_i. \tag{21}$$

Among these, the mass-diffusion term can be decomposed into three contributions as $\sigma_{diff}=\sigma_{Fi}+\sigma_{pd}+\sigma_{So}$, according to the components of Eq. (8), while the chemical term can be decomposed into separate contributions from each elementary reaction. It should be noted that the contribution from the 2nd term of the heat flux, Eq. (9), is included in the mass-diffusion component, Eq. (20). The last term of Eq. (9), the Dufour flux, was neglected in the calculations. However, the entropy generation due to the Dufour flux, Eq. (19), should equal that of the Soret flux, according to the Onsager reciprocal relations. Therefore, this neglected amount of entropy generation can be estimated by calculating that of the Soret flux. Entropy generation due to heat sources (including radiation) and body forces (e.g., gravity) was left out.

The chemical potential (Gibbs function) for each species is expressed as $g_i = h_i - Ts_i$. For ideal gases, $dh_i = C_{p,i}dT$ and $ds_i = (C_{p,i}/T)dT - (R_i/p_i)dp_i$, with $R_i = R_u/W_i$ and $p_i = X_i p$, hence

$$\left(\frac{1}{T}\frac{\partial h_i}{\partial x_\beta} - \frac{\partial s_i}{\partial x_\beta}\right) = \frac{R_i}{p_i}\frac{\partial p_i}{\partial x_\beta} = \frac{R_u}{W_i}\left(\frac{1}{X_i}\frac{\partial X_i}{\partial x_\beta} + \frac{1}{p}\frac{\partial p}{\partial x_\beta}\right) \tag{22}$$

The specific entropy is expressed as

$$s_i = s_i^\circ(T) - \frac{R_u}{W_i}\left(\ln X_i + \ln\frac{p}{p_{\text{ref}}}\right) \tag{23}$$

The temperature part $s_i^\circ(T)$, and the enthalpy $h_i(T)$, are determined from polynomials [46,47].

The chemical term, Eq. (21), contains the volumetric reaction rate for each species. With Eqs. (12) and (13), the term can be reformulated to provide the contribution of the jth elementary reactions as

$$\sigma_{\text{chem},j} = -\sum_{i=1}^{N_S}\frac{g_i}{T}W_i \cdot \nu_{ij} q_j. \tag{24}$$

The sum of these contributions will provide that of Eq. (21), $\sigma_{\text{chem}} = \sum_{j=1}^{N_R}\sigma_{\text{chem},j}$.

Exergy calculations

The exergy destruction rate was calculated as the product of the ambient temperature and the entropy generation rate, $T_0 \cdot \sigma$. The chemical exergy for H_2 was evaluated [4,48] to 238.16 kJ/mol for the ISO standard ambient air conditions for gas-turbine testing (15 °C, 1 atm, 60% relative humidity). In accordance with said standard, the ambient temperature was chosen as $T_0 = 288.15$ K. The calculation of chemical exergy at various ambient conditions was outlined by Ref. [4], and a comprehensive description and discussion of the accurate procedure was given by Ref. [48].

The DNS code and its assumptions

The S3D code is a massively parallel DNS solver developed at the Sandia National Labs, see Chen et al. [43]. It solves fully compressible momentum, total energy, species and mass continuity equations coupled with detailed chemistry. The code has been used for a wide range of studies of premixed (e.g. Refs. [3,49–51]) and non-premixed flames (e.g. Refs. [52–54]).

The transport equations were solved using an eighth-order explicit centered finite difference scheme in space (third-order one-sided stencils at the domain boundaries). A fourth-order six-stage explicit Runge-Kutta scheme was used for time integration [55]. Thermodynamic properties were modeled as polynomial functions of temperature and transport coefficients by the Chemkin and Transport packages [47,56].

The assumptions made in the S3D code were the ideal gas assumption for reactive fluid flow with continuum assumption for small length scales, body and buoyancy forces neglected, bulk viscosity neglected, a mixture-averaged diffusion coefficient used for all species, Dufour effect neglected, and no radiation heat transfer [43]. The Soret effect was implemented for light species (molar weight less than 5) [47], that is, H_2 and H.

Simulations of the head-on quenching flame

The present work made use of results from the previous studies, Salimath et al. [2], Gruber et al. [1]. The setup of the 1-dimensional cases is illustrated in Fig. 1. The flame front propagated in a premixed hydrogen/air mixture perpendicularly towards a solid wall facing the flame. The flame quenched when reaching the wall. Two configurations were investigated: a solid, impermeable wall (IW) and a hydrogen-permeable wall (PW). Both walls were chemically inert (no adsorption or catalytic effects). In the PW case, the flame became partly non-premixed, as H_2 seeped into the initial hydrogen-air mixture on the permeate side.

The numerical setup, models and boundary conditions are described previously, Salimath et al. [2]. Briefly outlined here, the domain had a length of $L = 0.02$ m, resolved in a uniform mesh of 4096 nodes and the time step fixed to $1.0 \cdot 10^{-9}$ s for all simulations. The air was assumed as 21% O_2 and 79% N_2, molar based. The chemical mechanism of Li et al. [57] was used, with 19 elementary reactions (Table 1) comprising 8 species (H_2, O_2, H_2O, OH, H, O, HO_2 and H_2O_2) in addition to inert N_2. The reactions are listed in Table 1, enumerated from R1 to R19. In the following, f and r will denote the forward and reverse net contributions of each reaction. The wall was assumed isothermal, and its temperature set equal to the unburnt-gas temperature, $T_w = T_u$. The pressure of the gas mixture was maintained at 1 atm. For the permeable wall, H_2 permeation occurred from $t = 0$.

It can be noted that for presentation purposes, results were extracted at every 1000 timesteps, i.e. at intervals of $1.0 \cdot 10^{-6}$ s. Furthermore, to provide correspondance with results from Ref. [2], the non-dimensional distance and time are used as $x^* = x/\delta_L$ and $t^* = t \cdot S_L^0/\delta_L$. Here, the laminar flame speed and thickness were used for the normalization.

The cases investigated had unburnt-mixture temperatures at 750 K, 500 K and 300 K, all with equivalence ratios at 0.5, 1.0 and 1.5. In addition, the stoichiometric cases at 750 K were diluted with nitrogen (two cases) and water vapour (two cases). All these 13 conditions were investigated for IW and for PW.

Results and discussion

Free propagating flame: verification and comparison

After initiation, the planar flame front moved undisturbed in the initially premixed fuel-air mixture. For a while, it behaved like a simple quasi-steady, 1-dimensional plane premixed flame. In our previous studies, it was seen that profiles from the undisturbed hydrogen-air [2] and methane-air [3] flames in S3D were virtually identical to results from Chemkin.

For comparison with previous work [10–12], the case of stoichiometric mixture and unburnt temperature 300 K was investigated.

Fig. 2 shows the spatial profiles of total entropy generation rate and its components due to chemical reactions, heat conduction and mass diffusion. The viscous contribution was

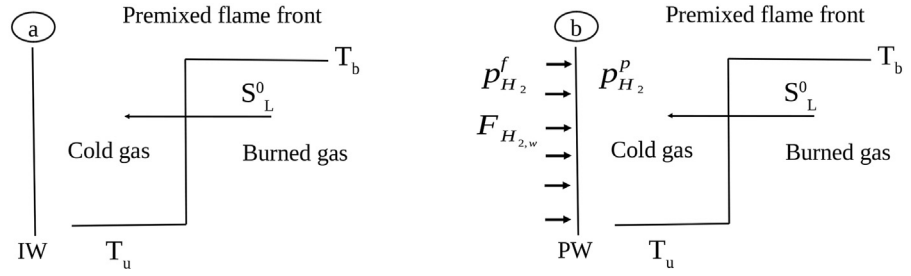

(a) Impermeable wall (IW) (b) Permeable wall (PW)

Fig. 1 – Head-on quenching configurations of impermeable and permeable walls with hydrogen flux.

Table 1 – Elementary reactions in the H_2–O_2 chemical mechanism, Li et al. [57].

No.	Reactions
R1	$O_2 + H \rightleftharpoons OH + O$
R2	$H_2 + O \rightleftharpoons OH + H$
R3	$OH + H_2 \rightleftharpoons H + H_2O$
R4	$H_2O + O \rightleftharpoons 2OH$
R5	$H_2 + M \rightleftharpoons 2H + M$
R6	$2O + M \rightleftharpoons O_2 + M$
R7	$H + O + M \rightleftharpoons OH + M$
R8	$OH + H + M \rightleftharpoons H_2O + M$
R9	$O_2 + H + M \rightleftharpoons HO_2 + M$
R10	$H + HO_2 \rightleftharpoons O_2 + H_2$
R11	$H + HO_2 \rightleftharpoons 2OH$
R12	$O + HO_2 \rightleftharpoons OH + O_2$
R13	$OH + HO_2 \rightleftharpoons O_2 + H_2O$
R14	$2HO_2 \rightleftharpoons O_2 + H_2O_2$
R15	$H_2O_2 + M \rightleftharpoons 2OH + M$
R16	$H + H_2O_2 \rightleftharpoons OH + H_2O$
R17	$H + H_2O_2 \rightleftharpoons H_2 + HO_2$
R18	$O + H_2O_2 \rightleftharpoons HO_2 + OH$
R19	$OH + H_2O_2 \rightleftharpoons H_2O + HO_2$

left out as it could not visually be distinguished from the zero line. Also the entropy diffusion is included (Eq. (15)).

These results were found to be within the results of the previous studies. The chemical and mass-diffusion components, normalized by the inflow fuel chemical exergy flow rate, were virtually identical to those of Zhang et al. [11], while our peak of the conductive component was larger, close to that of Nishida et al. [10]. The results of Acampora and Marra [12] seemed to be a little higher for all three components compared with our and the other results. The deviations may be attributed to differences in chemical mechanisms, transport models and numerical procedures.

Table 2 shows the quantities integrated spatially through the free propagating flame for some cases. Here, the chemical-reactions entropy generation is decomposed into the contributions from each of the 19 elementary reactions. Furthermore, the entropy generation due to mass diffusion is decomposed into the three components due to species gradient (Fick), pressure gradient and thermodiffusion (Soret).

In the table, the exergy destruction rate associated with the total entropy generation rate is also compared with the chemical exergy of the consumed hydrogen. The ratio of said quantities is included.

Head-on quenching

Fig. 3 shows the entropy generation and its components as function of time through quenching. For each timestep, the quantities were integrated over the length of the domain, $\int_0^L \sigma dx$. Also the integral of the diffusion, $\int_0^L B_s dx$ (Eq. (15)), is shown in the graphs.

The entropy generation due to reactions had a significant increase before the flame front reached the PW before fading off after quenching, while the IW case showed a gradual fade off.

The entropy generation of the most important elementary reactions are shown in Fig. 4. It is seen that the increase in the (overall) chemical component before quenching in the PW case was primarily due to reaction R8. Spikes from R5 and R8

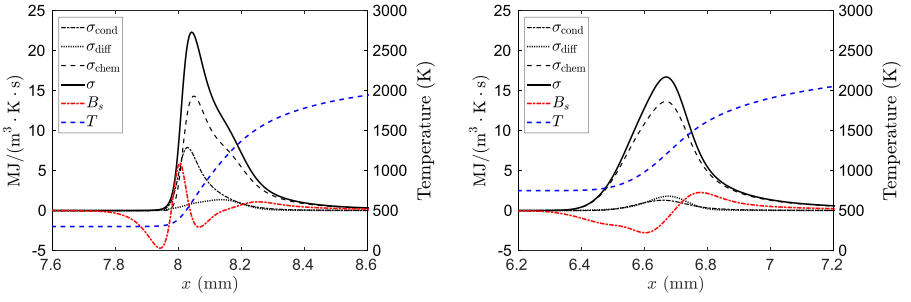

(a) $T_u = 300\,K$ (b) $T_u = 750\,K$

Fig. 2 – Components of entropy generation rate in the free propagating planar stoichiometric flame.

Table 2 – Components of entropy generation rate in a one-dimensional, quasi-steady planar H_2-air premixed flame (spatially integrated through the flame), fuel exergy and terms of the entropy equation.

ϕ_u (–)	1.0	1.0	0.5	1.5
T_u (K)	300	750	750	750
Total entropy generation rate (kW/(m^2 K))	3.825	4.595	2.316	5.421
Heat conduction (fraction of total)	0.241	0.0615	0.0571	0.0636
Mass diffusion (of total)	0.0719	0.0698	0.0642	0.0702
Chemical reactions (of total)	0.687	0.869	0.879	0.866
Viscous forces (of total)	$3.2 \cdot 10^{-6}$	$5.4 \cdot 10^{-6}$	$2.3 \cdot 10^{-6}$	$6.2 \cdot 10^{-6}$
Species gradient (fraction of mass diffusion)	0.922	0.962	0.953	0.973
Pressure gradient (fraction of mass diffusion)	$1.08 \cdot 10^{-5}$	$4.4 \cdot 10^{-5}$	$1.7 \cdot 10^{-5}$	$4.6 \cdot 10^{-5}$
Thermal (Soret) (fraction of mass diffusion)	0.078	0.038	0.0475	0.0266
R1 (fraction of chem. Component)	0.0170	0.0318	0.0146	0.0501
R2	0.0208	0.0332	0.0262	0.0402
R3	0.117	0.162	0.160	0.164
R4	$9.9 \cdot 10^{-4}$	$3.6 \cdot 10^{-4}$	$9.8 \cdot 10^{-4}$	$2.0 \cdot 10^{-4}$
R5	0.0167	0.0305	0.101	0.0566
R6	$3.3 \cdot 10^{-4}$	$5.7 \cdot 10^{-4}$	$1.3 \cdot 10^{-3}$	$1.6 \cdot 10^{-4}$
R7	0.0276	0.0490	0.0387	0.0385
R8	0.231	0.289	0.193	0.288
R9	0.247	0.174	0.236	0.156
R10	0.0312	0.0258	0.0316	0.0235
R11	0.203	0.176	0.207	0.167
R12	0.0120	$9.3 \cdot 10^{-3}$	0.0312	0.0049
R13	0.0686	0.0126	0.0381	0.0070
R14	$6.4 \cdot 10^{-4}$	$3.9 \cdot 10^{-4}$	$9.6 \cdot 10^{-5}$	$3.1 \cdot 10^{-5}$
R15	0.00125	$8.2 \cdot 10^{-4}$	$1.6 \cdot 10^{-3}$	$4.0 \cdot 10^{-4}$
R16	$3.02 \cdot 10^{-3}$	$2.5 \cdot 10^{-3}$	$2.8 \cdot 10^{-3}$	$1.6 \cdot 10^{-3}$
R17	$4.1 \cdot 10^{-4}$	$5.9 \cdot 10^{-4}$	$4.8 \cdot 10^{-4}$	$3.9 \cdot 10^{-4}$
R18	$2.2 \cdot 10^{-4}$	$3.3 \cdot 10^{-4}$	$8.3 \cdot 10^{-4}$	$6.4 \cdot 10^{-5}$
R19	$1.98 \cdot 10^{-3}$	$2.2 \cdot 10^{-3}$	$4.6 \cdot 10^{-3}$	$5.9 \cdot 10^{-4}$
Fuel exergy converted (kW/m^2)	5337	11,375	4311	12,637
Exergy destruction ratio (–)	0.207	0.127	0.155	0.124
Entropy transient term (kW/(m^2 K))	−11.77	−23.5	−12.6	−26.2
Entropy convection rate (kW/(m^2 K))	15.59	28.1	15.0	31.6
Entropy diffusion rate (kW/(m^2 K))	0.0035	−0.0016	$-2.3 \cdot 10^{-5}$	0.0050
Entropy generation rate (kW/(m^2 K))	3.825	4.595	2.316	5.421

were counteracted by decrease in other reactions and were not visible in the chemical component, Fig. 3b.

Heat-conduction entropy generation had a notable increase through the quenching, and became the largest contribution after quenching. The mass diffusion contribution diminished to a negligible value for IW. For PW, the H_2 permeation caused some entropy generation also after quenching. The contribution from viscous forces was evaluated, but not included in the graphs, as the curves were not visibly distinguishable from zero. At quenching (t^*_Q), the non-dimensional viscous entropy generation σ^*_{visc} (cf. Fig. 3) had values of $2.2 \cdot 10^{-4}$ for IW and $6.9 \cdot 10^{-7}$ for PW.

The mass diffusion has three components (Eq. (8)). Their contributions are shown in Fig. 5. The pressure diffusion was very small due to a nearly constant pressure. The contribution of the Soret diffusion can be of particular interest, since it is usually neglected. The computations confirmed that the Soret entropy generation was very small. Just after quenching for PW, it peaked to 0.008 times the free-flame total entropy generation. Its contribution to the total entropy generation remained less than 1% for all times throughout quenching for PW and had a lesser contribution for IW.

When the flame approached the wall, the Soret entropy generation showed negative values. This was caused by a combination of a positive temperature gradient (negative Soret flux) and negative species gradients (primarily H_2). Negative contribution to entropy generation by the Soret effect was also observed by Torabi et al. [58]. It should be noted that a positive total entropy generation was maintained also at these instances.

Although the Dufour effect was not implemented in the code, its contribution to entropy generation can be evaluated from that of the Soret effect, which is of equal value.

The entropy diffusion components, Eq. (15), due to heat conduction and mass diffusion, respectively, had opposite signs. Both increased considerably towards the quenching instance, and then decreased. Since their relative weights were different for PW and IW, the resulting total entropy diffusion B_s had different signs for the two configurations, as seen in Fig. 3.

It was noted that the IW results showed a small, but marked step at $t^* = 547.1$. Since it ocurred well after the quenching instance, we did not make further investigations. However, it was observed that at this instance, the flow velocity was reduced towards zero in most of the domain and had changed direction close to the wall.

The detailed temporal development of the entropy generation and its main components through quenching is shown in Fig. 6 for PW. Contributions from selected elementary reactions are shown in Fig. 7. It can be noted that the ordinates of these graphs are dimensional, while the non-dimensional distance and time are retained from Ref. [2] for easier comparison. The corresponding results for IW are shown in Figs. 8 and 9. It was seen that the diffusion contribution became lower, both absolutely and relatively, when the flame came close to the wall. Hence, the species concentrations gradients were reduced towards quenching.

Effects of fuel-air ratio

The investigations were conducted for a lean ($\phi_u = 0.5$) and a rich ($\phi_u = 1.5$) mixture, in addition to the stoichiometric cases in the preceding section. The total entropy generation rate and its components were integrated over the spatial domain, $\int_0^L \sigma(x,t)dx$, as described above. This transient quantity was then multiplied

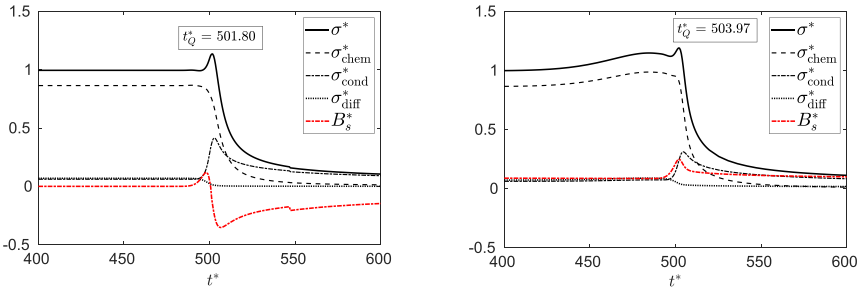

(a) Impermeable wall (IW) (b) Permeable wall (PW)

Fig. 3 – Entropy generation rate components and entropy diffusion integrated over the length of the domain as a function of time, $\phi_u = 1.0$, $T_u = 750$ K. Values are made non-dimensional with the integral of the total entropy generation through the free propagating flame.

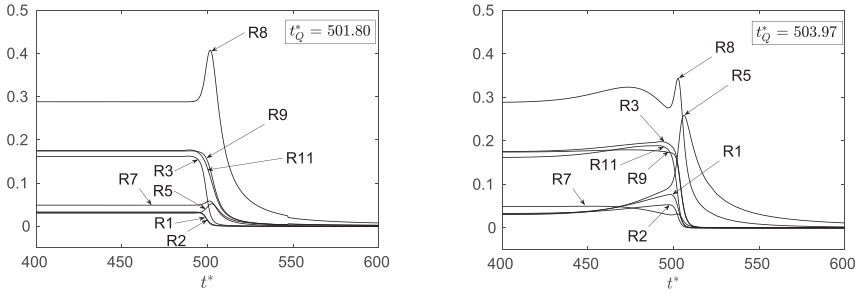

(a) Impermeable wall (IW) (b) Permeable wall (PW)

Fig. 4 – Entropy generation rate components due to some elementary reactions, integrated over the length of the domain as a function of time, $\phi_u = 1.0$, $T_u = 750$ K. Values are made non-dimensional with the integral of the total entropy generation through the free propagating flame.

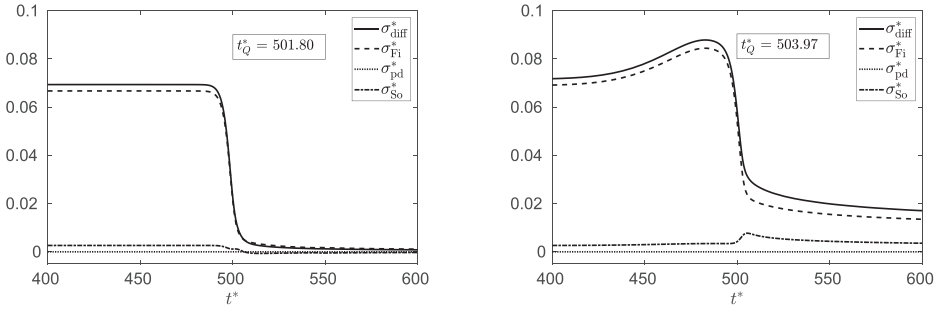

(a) Impermeable wall (IW) (b) Permeable wall (PW)

Fig. 5 – Entropy generation rate due to mass diffusion and its components integrated over the length of the domain as a function of time, permeable wall, $\phi_u = 1.0$, $T_u = 750$ K. Values are made non-dimensional with the integral of the total entropy generation through the free propagating flame.

with the ambient temperature, T_0, to provide the exergy destruction rate (ED) in the domain at each timestep. These results are shown in Fig. 10. Also shown is the rate of conversion of H_2 chemical exergy (CE), that is, $\varepsilon^{ch}_{H_2} \cdot \int_0^L (-\dot{\omega}_{H2}(x,t))dx$. This comparison was found relevant, since IW and PW had different amounts of fuel, due to permeation through the wall. Although H_2 alone did not give the complete image of the chemical conversion, it gave a clear indication. For a comparison between the different mixtures, the integrated rates are shown as dimensional quantities. For convenience, the chemical-exergy conversion rates were scaled by a factor of 0.2 in the graphs.

As observed previously [1,2], the conductive heat flux for the IW configuration varied notably with the equivalence ratio near quenching. This also led to a strong variation in the corresponding entropy generation rate. As seen in Fig. 10a for the rich case, the conduction component was the largest contributor at quenching. For the stoichiometric and lean IW cases, this component was notably smaller, both relatively

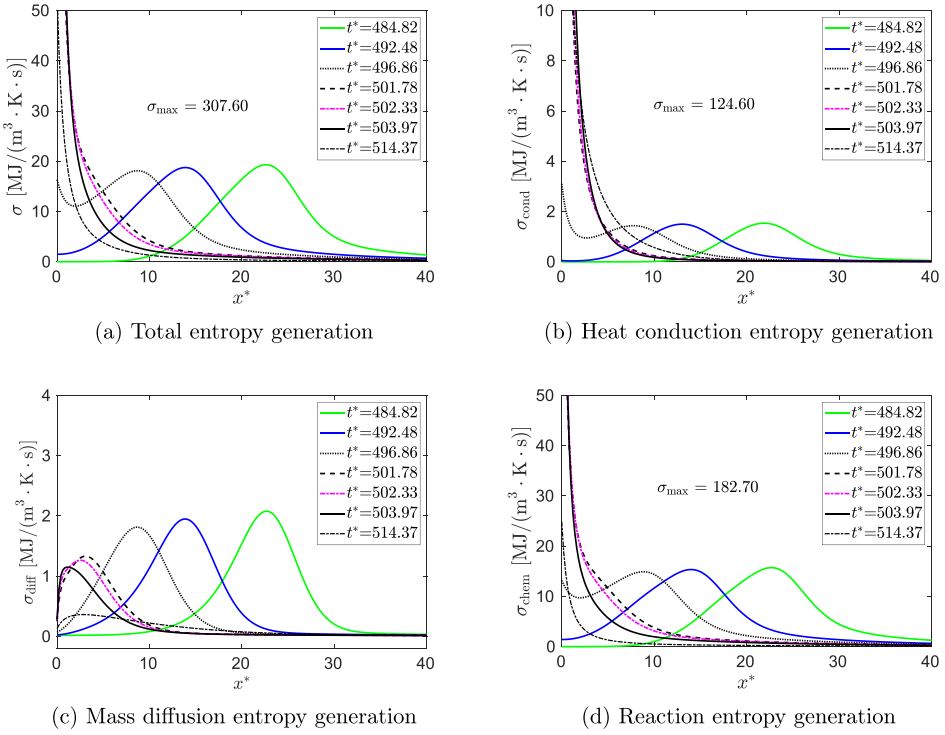

(a) Total entropy generation (b) Heat conduction entropy generation

(c) Mass diffusion entropy generation (d) Reaction entropy generation

Fig. 6 – Entropy generation rates vs. distance from wall for various time. Permeable wall, $\phi_u = 1.0$, $T_u = 750$ K.

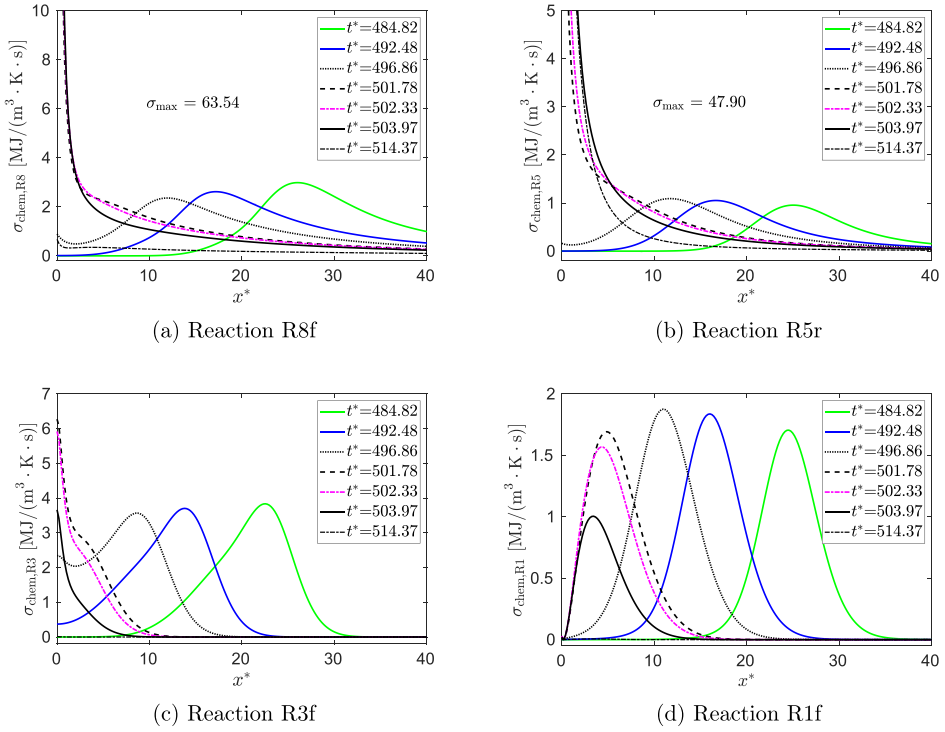

(a) Reaction R8f (b) Reaction R5r

(c) Reaction R3f (d) Reaction R1f

Fig. 7 – Entropy generation rates vs. distance from wall for various time for selected elementary reactions. Permeable wall, $\phi_u = 1.0$, $T_u = 750$ K.

and absolutely. While the conduction component peaked, the chemical and diffusive components just faded off at quenching for all stoichiometries.

For the PW configuration, the peak of conductive heat flux at quenching did not show much variation with equivalence ratio. It was slightly reduced with increasing

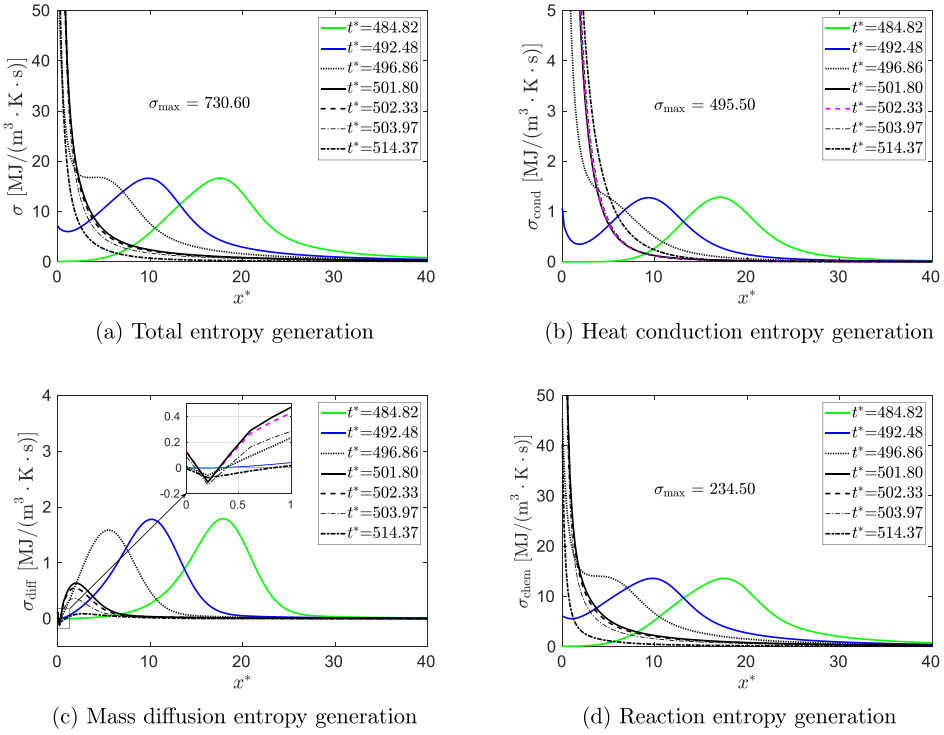

(a) Total entropy generation (b) Heat conduction entropy generation

(c) Mass diffusion entropy generation (d) Reaction entropy generation

Fig. 8 – Entropy generation rates vs. distance from wall for various time. Impermeable wall, $\phi_u = 1.0$, $T_u = 750$ K.

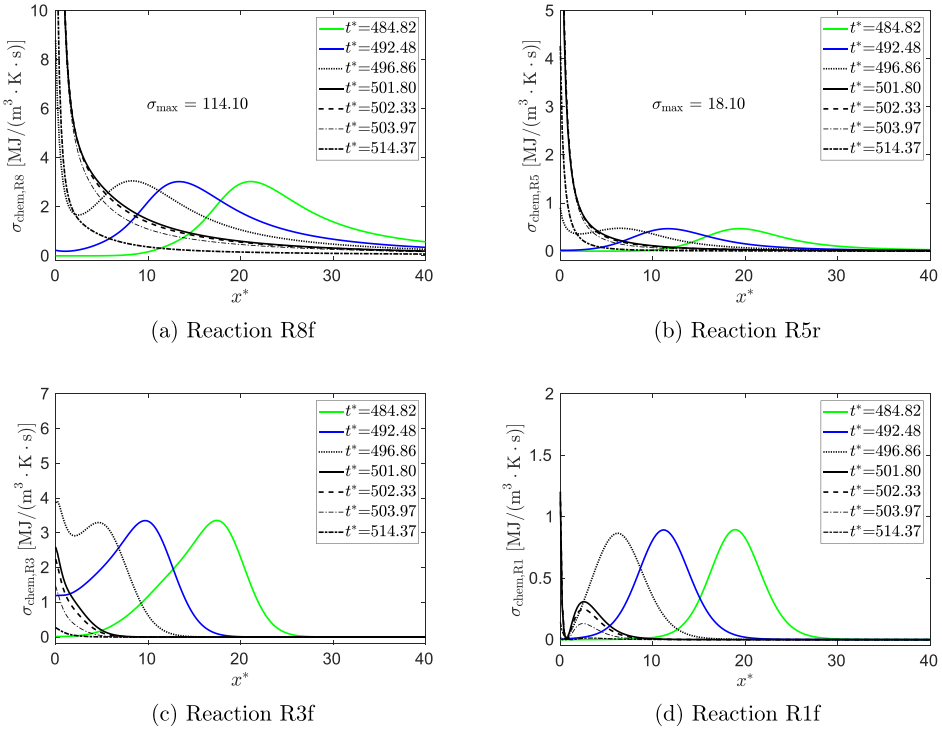

(a) Reaction R8f (b) Reaction R5r

(c) Reaction R3f (d) Reaction R1f

Fig. 9 – Entropy generation rates vs. distance from wall for various time for selected elementary reactions. Impermeable wall, $\phi_u = 1.0$, $T_u = 750$ K.

equivalence ratio, similar to the wall heat flux (displayed in Ref. [1]). On the other hand, the chemical component of entropy generation showed more variation, in particular, between the lean case and the stoichiometric and rich cases. For the lean case, and to some extent the stoichiometric case, a higher content of fuel close to the hydrogen-permeable wall led to an increased chemical conversion and more entropy generation. Therefore, the chemical

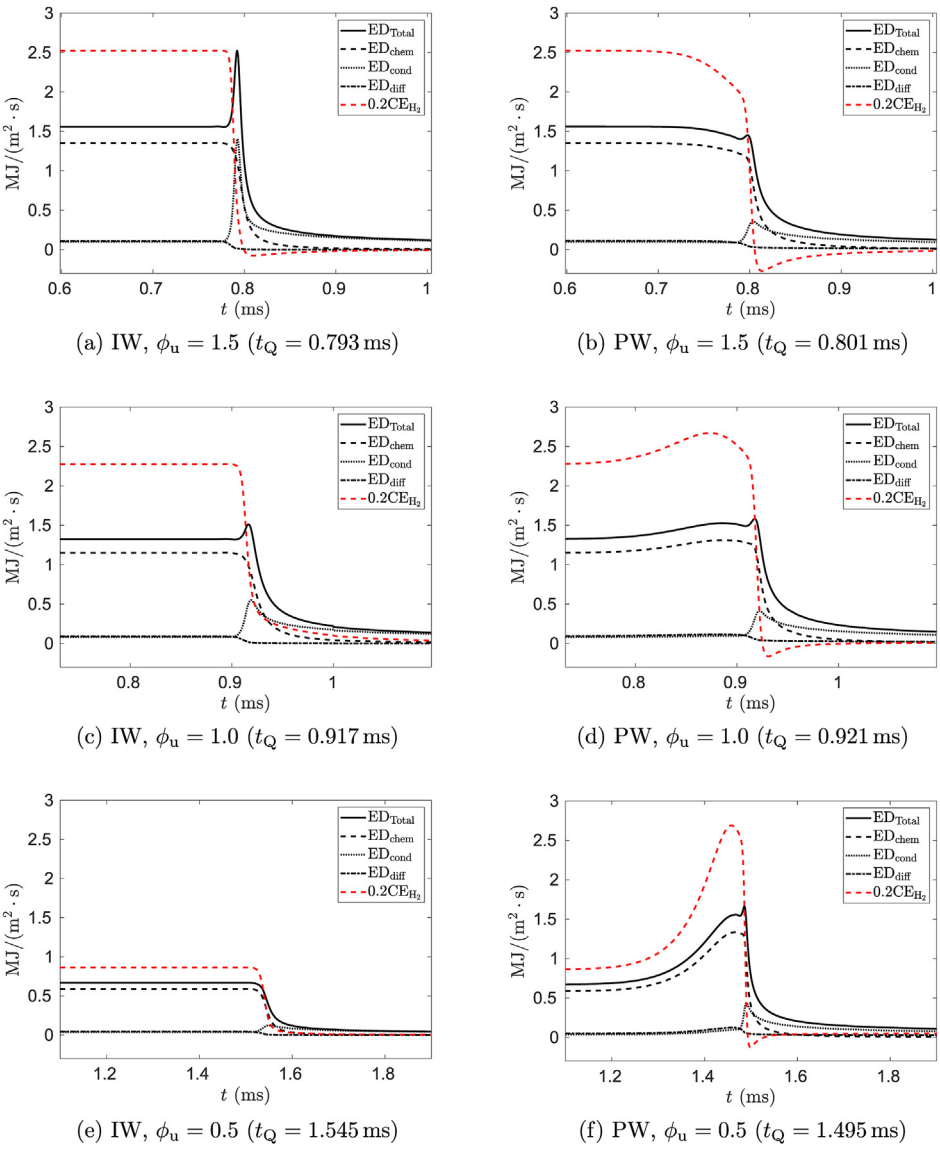

(a) IW, $\phi_u = 1.5$ ($t_Q = 0.793$ ms) (b) PW, $\phi_u = 1.5$ ($t_Q = 0.801$ ms)

(c) IW, $\phi_u = 1.0$ ($t_Q = 0.917$ ms) (d) PW, $\phi_u = 1.0$ ($t_Q = 0.921$ ms)

(e) IW, $\phi_u = 0.5$ ($t_Q = 1.545$ ms) (f) PW, $\phi_u = 0.5$ ($t_Q = 1.495$ ms)

Fig. 10 – Exergy destruction (ED) rate components and hydrogen chemical exergy conversion (CE) rate (notice scale), integrated over the length of the domain as a function of time for $T_u = 750$ K and different equivalence ratios.

component of entropy generation increased as the flame approached the wall. Close to the quenching instance, the chemical component of these cases also decreased and eventually faded off. In comparison, the conductive component had a slower fade off after quenching, and it became the biggest contributor to entropy generation in the weakly reacting mixture after quenching.

For all these cases, the already modest diffusive component of entropy generation faded off before quenching.

Inspecting the contributions of individual elementary reactions, the overall view was to some extent similar to the stochiometric case, Fig. 4. However, some deviations were noted. For the free propagating flame, the rich case was not very different from the stoichiometric. The most important reaction was R8f, followed by R11f, R3f and R9f. Also R5r, R1f and R2f had notable contributions. All these reactions had a moderately larger entropy generation in the rich case. In the lean case, the contributions were considerably lesser. In particular, R8 was reduced to one-third compared to stoichiometric case, falling below R9 and R11.

When the flame approached the impermeable wall (IW) for the rich case, R8 and R5 had spikes similar to the stoichiometric case. The other chemical contributions declined before these spikes, and the sum of chemical contributions faded off, as seen in Fig. 10a. For the lean case, all important reactions just faded off.

For the permeable wall (PW) rich case, R8 began decreasing some time before quenching, before it got a peak close to quenching. For the other reactions, the behaviour was similar to that of the stoichiometric case. In the lean case, the reactions mentioned (R11f, R3f, R9f, R5r, R1f, R2f) had an increase when the flame approached the wall. In particular, R8 rose to a level like that of the stoichiometric case. For all PW

cases, and to lesser extent the rich IW case, R5 showed a strong increase in entropy generation just before quenching, when other reactions decreased. For these cases, R5 remained the largest contributor after quenching, although at a much lower level. The negative H_2 consumption seen in Fig. 10 can be associated with the reverse R5 recombining 2H into H_2.

As noted in the Introduction, previous studies on non-premixed and some partially premixed flames had found the conduction to be the largest contributor to entropy generation. For premixed flames, chemical reactions have been found to dominate. On this background, it is worth noting that the permeation of hydrogen from the wall, i.e. a non-premixed supply of fuel, can increase the weight of the chemical reactions in entropy generation.

Effects on the entropy diffusion flux B_s, Eq. (15), are shown in Fig. 11 presented as $\int_0^L B_s dx$. As in Fig. 4, the values were made non-dimensional with the integral of the total entropy generation through the free propagating stoichiometric flame. It was seen that the entropy flux was virtually zero in the free propagating flame (cf. Table 2). For IW, the lean flame had a flux towards the wall (i.e. negative) when approaching quenching. With increasing fuel-air ratio, a period with positive flux appeared shortly before quenching. In the $\phi_u = 1.5$ case, this became the main effect. For PW, the permeating fuel gave a positive (non-zero) entropy flux near the wall for the entire period, with a strong increase just before quenching.

For an overall comparison, the spatially integrated exergy destruction rate was also integrated for a time interval ending at the quenching instance:

$$\mathrm{ED} = T_0 \int_{t_1}^{t_Q} \int_0^L \sigma(x,t) dx dt \tag{25}$$

For PW, the integral was taken from the time t_1, where the wall permeation began affecting the flame (beginning of "Stage II", cf [2]). For IW, t_1 was chosen so that the time interval $(t_Q - t_1)$ had the same value for each pair of IW and PW cases. The exergy destruction, Eq. (25), can be compared with the exergy of the converted fuel in the same interval, $\mathrm{CE} = \varepsilon^{ch}_{H2} \cdot \int_{t_1}^{t_Q} \int_0^L (-\dot{\omega}_{H2}(x,t)) dx dt$.

The fraction of entropy generation due to conduction increased for IW with increasing equivalence ratio, from 5.9% for $\phi_u = 0.5$ and 6.7% for $\phi_u = 1.0$, to 10% for $\phi_u = 1.5$. The diffusion fraction had a maximum at 7.1% at stoichiometric conditions, with a small reduction for rich and lean. The chemistry dominated (≈86%) and had a slightly reduced share with increasing equivalence ratio. Compared with the H_2 chemical exergy conversion (CE), Fig. 12, all components of exergy destruction had a minimum at stoichiometric conditions. The conduction and diffusion components had small increases for rich and lean mixtures, while the chemical term increased most notably for lean conditions. For the PW configuration, the variations were similar to, but less than those of IW.

From Eq. (18), showing σ_{cond} inversely proportional to the square of the temperature, an increase in this component was expected at a reduced temperature. On the contrary, the diffusion component, Eqs. (20) and (22), does not have a direct relation to temperature. The chemical component, Eq. (21), is inversely proportional to the temperature, and proportional to the reaction rate involving an exponential function. The latter relation will also affect the fuel conversion. Since the reaction Gibbs energy difference varies more with temperature than the corresponding enthalpy difference, the entropy generation variation differs from that of the heat release.

Our previous results [1,2] showed that for IW, the lean flame had lower temperatures, while the rich flame had approximately

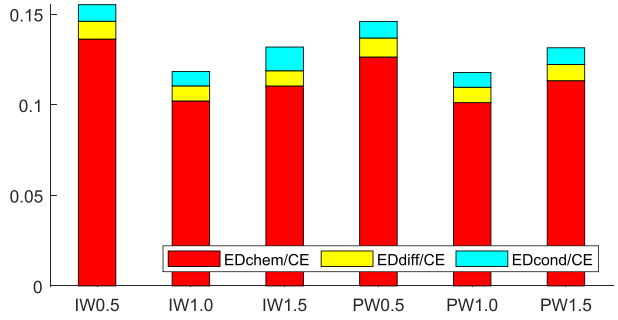

Fig. 12 – Effect of equivalence ratio: Components of exergy destruction (ED) in the domain for a time interval up to quenching as fractions of the converted fuel chemical exergy (CE), $T_u = T_w = 750$ K.

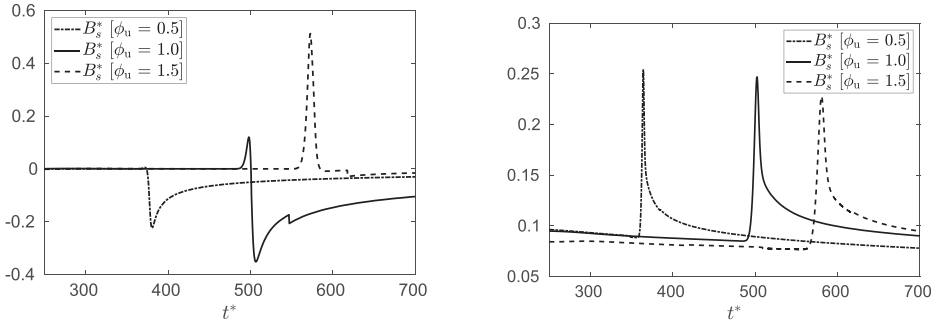

(a) IW (b) PW

Fig. 11 – Entropy diffusion rate integrated over the length of the domain as a function of time, $T_u = 750$ K at different equivalence ratios. Values are made non-dimensional with the integral of the total entropy generation through the free propagating flame for $\phi_u = 1.0$.

the same temperatures as the stoichiometric. For PW, the permeation led to a higher local equivalence ratio close to the wall. The (initially) lean and stoichiometric mixtures gave similar temperatures, while the rich flame got lower values. Compared to IW, the lean PW case had higher temperatures, the stoichiometric case was on par with IW, while for the rich mixture the temperatures were lower than for IW.

The entropy generation caused by the isothermal expansion of H_2 through the membrane, from the feed pressure (10 atm) to the partial pressure on the permeate side, was not included in the results above. It was estimated to approximately 1% of the total entropy generation.

Effects of mixture temperature

Both configurations, with rich, stoichiometric and lean mixtures, were computed with temperatures of the unburnt mixture and the wall ($T_u = T_w$) at 500 K and 300 K [2].

The exergy destruction for the domain and the time interval was compared with the chemical exergy of the converted fuel, as described above. The results are shown in Fig. 13. It was seen that lower temperatures gave larger values both for the total and the components of exergy destruction. The fraction due to diffusion was slightly larger at lower temperatures, while the conduction fraction of total entropy generation increased considerably (from 7% at 750 K to 25% at 300 K, stoichiometric). The variations with equivalence ratio were similar to those at the higher temperature in the preceding section.

Effects of dilution with nitrogen or water vapour

The stoichiometric cases at 750 K (Case D0, IW and PW as above) were diluted by increasing the unburnt-mixture nitrogen-oxygen molar ratio from 3.762 (undiluted Case D0, with no H_2O) to 4.0 (Case D1) and 4.762 (Case D2), for both configurations. Furthermore, water vapour was added such that the H_2O–O_2 ratio of the unburnt mixture increased from zero (Case D0) to 0.12 (Case D3) and 3.147 (Case D4), as described in Ref. [2].

Basically, dilution will reduce the reaction temperatures and the effects can be expected similar to those of the reduced temperature in the preceding section.

The exergy destruction integrated over the domain and the time interval was compared with the chemical exergy of the converted fuel, as described above. The results are shown in Fig. 14.

Dilution with (inert) N_2 (Cases D1 and D2) gave modest increases in total exergy destruction as fraction of converted fuel exergy and in the chemical component. Dilution with H_2O had a different effect for the smaller amount (Cases D3). Then, the chemical component (relative to converted fuel exergy) was reduced. The reasons seemed to be that some additional H_2O gave an increased conversion of fuel (H_2). Further dilution with more vapour (Cases D4) had the same effect as dilution with N_2, i.e. modest increases. The effects were similar for both configurations.

Permeable vs. impermeable wall

The entropy generation primarily followed inversely the temperature. Lower unburnt-mixture temperature, deviation from stoichiometry and dilution all gave lower temperatures and higher total entropy generation and exergy destruction per unit of converted fuel.

The effects of fuel permeation were more complex. It had a cooling effect close to the wall due to thermal dilution [1,3]. Entering a lean mixture, additional fuel gave increased fuel conversion and a higher temperature near the wall. The higher temperature due to reaction heat release was more pronounced on entropy generation than the cooling effect. When fuel permeated into an initially stoichiometric or rich mixture, the local mixture became richer. Therefore, the temperature was lowered, and the entropy generation increased.

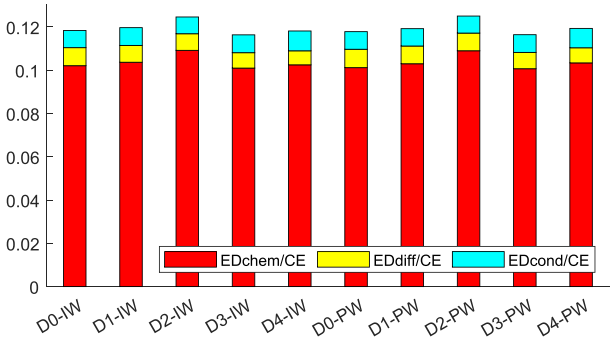

Fig. 14 – Effect of dilution: Components of exergy destruction (ED) in the domain for a time interval up to quenching as fractions of the correspondingly converted fuel chemical exergy (CE).

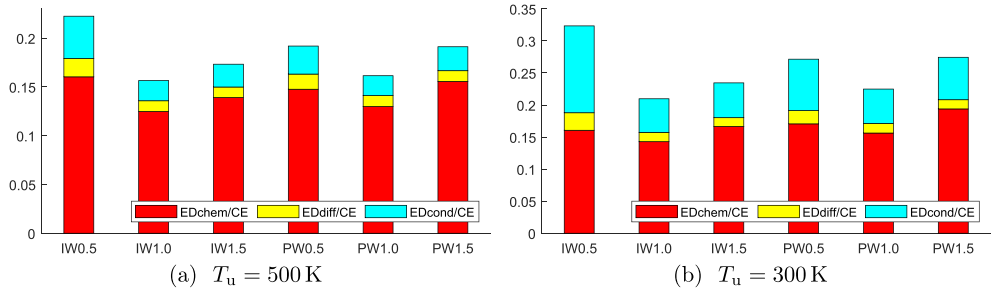

Fig. 13 – Effect of unburnt temperature: Components of exergy destruction (ED) in the domain for a time interval up to quenching as fractions of the correspondingly converted fuel chemical exergy (CE).

The main contributions to entropy generation were reactions and conduction. Diffusion had, in general, a minor impact. Even though permeation influenced diffusion, the effect of this on entropy generation was small.

The investigations of permeable walls are motivated by, among other, potential emissions reduction and efficiency improvement. The permeation zone will be a smaller part of a combustor. When incomplete fuel conversion occurs, it will be a localized phenomenon, and the conversion can be completed elsewhere in the combustor. Accordingly, the primary interest will be to observe the entropy generation per unit of converted fuel. Permeating fuel increased the entropy generation because the fuel conversion increased. The entropy generation per unit of converted fuel was either decreased (lean mixtures) or marginally affected (stoichiometric or rich mixtures) by permeation.

Conclusions

Previous investigations [1,2] on 1-D head-on premixed H_2-air flame interacting with an impermeable wall (IW) or a permeable wall (PW) were extended with computations of entropy generation and entropy fluxes. Additional fuel was supplied through the permeable wall.

In general, fuel permeation through the wall increased both entropy generation and fuel conversion.

The permeating fuel had a diversity of effects. First, it had a cooling effect close to the wall. Separately, this thermal dilution reduced the local temperature and contributed to increased entropy generation. However, for initially lean and stoichiometric mixtures, the additional fuel provided more reaction heat release, leading to higher temperature and reduced entropy generation per unit of converted fuel. Permeation also increased the mass flux, and thereby the entropy flux, away from the wall. The effects of mass diffusion on entropy generation were modest, and the altered mass diffusion made small changes from IW to PW. The Soret diffusion (thermodiffusion) had small contribution to the mass diffusion entropy generation. During quenching it became even smaller for IW, while it had an increase for PW. The effects of pressure diffusion were negligible.

The effects of permeation were similar for all unburnt-temperatures investigated (750 K, 500 K, 300 K). As expected from theory and other studies, a lower temperature gave higher entropy generation. Furthermore, in accordance with literature, the chemical reaction gave the major part of entropy generation, with conduction as the second most important source. Mass diffusion was of modest importance, while viscous forces had vanishing effects.

Permeation to a lean mixture reduced entropy generation per unit of fuel converted. The effect was stronger for lower temperatures because then the conduction had a greater share of the total entropy generation. At the higher unburnt-mixture temperature, similar results were seen for rich mixtures, as well. For the lower temperature, permeation into a rich mixture increased the entropy generation per unit of converted fuel.

The elementary reactions most important for entropy generation towards quenching were R8 ($OH + H + M \rightleftharpoons H_2O + M$, net forward), R5 ($H_2 + M \rightleftharpoons 2H + M$, net reverse) and R3 ($OH + H_2 \rightleftharpoons H + H_2O$, net forward). In particular, the recombining R5r had a notable relative increase towards the quenching instance. Both R8f and R5r had high peaks of entropy generation rate when the flame reached the wall and quenched.

Declaration of competing interest

The authors declare that they have no known competing financial interests or personal relationships that could have appeared to influence the work reported in this paper.

Acknowledgments

We are grateful to the Norwegian e-infrastructure for Research and Education (Uninett Sigma2 AS) for providing the HPC computational resources and useful technical support (project No. NN9400K).

Nomenclature

A_j	factor in reaction-rate model, reaction j
B_s	entropy diffusion term (J/(s•m^3•K))
C_p, $C_{p,i}$	specific heat capacity at constant pressure (for species i) (J/(kg•K))
$d_{\alpha i}$	diffusion driving force of species i in x_α direction (m^{-1})
D_i^{mix}	mixture-averaged mass diffusivity of species i (m^2/s)
D_i^T	thermal diffusion coefficient of species i (kg/(ms))
e	specific internal energy (J/kg)
E_j	activation energy in reaction j (J/(mol•K))
g_i	specific chemical potential (Gibbs function) for species i (J/kg)
h_i	specific enthalpy for species i (J/kg)
$J_{\alpha i}$	diffusive mass flux of species i in x_α direction (kg/(s•m^2))
k_{fj}, k_{fj}	forward, reverse rate coefficients of reaction j
K_{cj}	equilibrium constant of reaction j (–)
L	length of domain (m)
N_R	number of reactions (–)
N_S	number of species (–)
p, p_{ref}	pressure, reference pressure (Pa)
q_j	reaction progress of elementary reaction j (mol/(m^{3}s))
q_α	heat flux in x_α direction (J/(s •m^2))
R_u	universal gas constant (J/(mol•K))
s, s_i	specific entropy (J/(kg•K))
s_i°	specific entropy at reference pressure (J/(kg•K))
S_L^0	laminar flame speed (m/s)
t	time (s)
T, T_0	temperature, ambient temperature (K)
u_α	velocity component in x_α direction (m/s)
$V_{\alpha i}$	mass diffusion velocity of species i in x_α direction (m/s)
W_i	molar mass of species i (kg/kmol)
x, x_α	spatial coordinate (m)

X_i	mole fraction of species i (–)
Y_i	mass fraction of species i (–)
β_j	exponent in reaction-rate model, reaction j (–)
$\delta_{\alpha\beta}$	Kronecker delta (–)
δ_L	Laminar flame thickness (m)
ε_i^{ch}	chemical specific exergy for species i (kJ/kg)
λ	thermal conductivity (J/(s•m•K))
μ	viscosity (Pa•s)
ν_{ij}	reaction coefficient of species i in reaction j (–)
ν'_{ij}, ν''_{ij}	reaction coefficients of species i (reactant, product) in reaction j (–)
ρ	mass density (kg/m^3)
σ	volumetric entropy generation rate (J/(s•m^3•K))
$\tau_{\alpha\beta}$	viscous stress tensor (Pa)
ω_i	volumetric molar reaction rate of species i (mol/(m^{3}s))

Superscripts/Subscripts

*	non-dimensional
Du	Dufour
Fi	Fick (species gradient diffusion)
Fo	Fourier (thermal gradient conduction)
J	mass diffusion
pd	pressure diffusion
Q	quenching
So	Soret

REFERENCES

[1] Gruber A, Salimath PS, Chen JH. Direct numerical simulation of laminar flame-wall interaction for a novel H2-selective membrane/injector configuration. Int J Hydrogen Energy 2014;39(11):5906–18. https://doi.org/10.1016/j.ijhydene.2014.01.148.

[2] Salimath PS, Ertesvåg IS, Gruber A. Premixed hydrogen–air flames interacting with a hydrogen porous wall. Int J Hydrogen Energy 2018;43(7):3822–36. https://doi.org/10.1016/j.ijhydene.2017.12.166.

[3] Salimath PS, Ertesvåg IS, Gruber A. Computational analysis of premixed methane-air flame interacting with a solid wall or a hydrogen porous wall. Fuel 2020;272:117658. https://doi.org/10.1016/j.fuel.2020.117658.

[4] Szargut J, Morris DR, Steward FR. Exergy analysis of thermal, chemical, and metallurgical processes. New York: Hemisphere; 1988.

[5] Kotas TJ. The exergy method for thermal plant analysis. London, UK: Butterworths; 1985.

[6] Rian AB, Ertesvåg IS. Exergy analysis of a steam production and distribution system including alternatives to throttling and the single pressure steam production. Energy Convers Manag 2011;52(1):703–12. https://doi.org/10.1016/j.enconman.2010.07.049.

[7] Ertesvåg IS. Exergy calculations based on a fixed standard reference environment vs. the actual ambient conditions: gas turbine and fuel cell examples. Int J Exergy 2015;16(2):239–61. https://doi.org/10.1504/IJEX.2015.068209.

[8] Som SK, Datta A. Thermodynamic irreversibilities and exergy balance in combustion processes. Prog Energy Combust Sci 2008;34(3):351–76. https://doi.org/10.1016/j.pecs.2007.09.001.

[9] Arpaci VS, Selamet A. Entropy production in flames. Combust Flame 1988;73(3):251–9. https://doi.org/10.1016/0010-2180(88)90022-3.

[10] Nishida K, Takagi T, Kinoshita S. Analysis of entropy generation and energy loss during combustion. Proc Combust Inst 2002;29(1):869–74. https://doi.org/10.1016/S1540-7489(02)80111-0.

[11] Zhang J, Han D, Huang Z. Second-law thermodynamic analysis for premixed hydrogen flames with diluents of argon/nitrogen/carbon dioxide. Int J Hydrogen Energy 2019;44(10):5020–9. https://doi.org/10.1016/j.ijhydene.2019.01.041.

[12] Acampora L, Marra FS. Second law thermodynamic analysis of syngas premixed flames. Int J Hydrogen Energy 2020;45(21):12185–202. https://doi.org/10.1016/j.ijhydene.2020.02.142.

[13] Liu D, Wang H, Zhang Y, Liu H, Zheng Z, Yao M. On the entropy generation and exergy loss of laminar premixed flame under engine-relevant conditions. Fuel 2021;283:119245. https://doi.org/10.1016/j.fuel.2020.119245.

[14] Chen S. Analysis of entropy generation in counter-flow premixed hydrogen-air combustion. Int J Hydrogen Energy 2010;35(3):1401–11. https://doi.org/10.1016/j.ijhydene.2009.11.080.

[15] Jejurkar SY, Mishra DP. Effects of wall thermal conductivity on entropy generation and exergy losses in a H2-air premixed flame microcombustor. Int J Hydrogen Energy 2011;36(24):15851–9. https://doi.org/10.1016/j.ijhydene.2011.08.116.

[16] Jejurkar SY, Mishra DP. Numerical analysis of entropy generation in an annular microcombustor using multistep kinetics. Appl Therm Eng 2013;52(2):394–401. https://doi.org/10.1016/j.applthermaleng.2012.12.021.

[17] Jiang D, Yang W, Chua KJ. Entropy generation analysis of H2/air premixed flame in microcombustors with heat recuperation. Chem Eng Sci 2013;98:265–72. https://doi.org/10.1016/j.ces.2013.05.038.

[18] Li Z, Chou S, Shu C, Yang W. Entropy generation during microcombustion. J Appl Phys 2005;97(8):084914. https://doi.org/10.1063/1.1876573.

[19] Jiang D, Yang W, Teng J. Entropy generation analysis of fuel lean premixed CO/H2/air flames. Int J Hydrogen Energy 2015;40(15):5210–20. https://doi.org/10.1016/j.ijhydene.2015.02.082.

[20] Zuo W, Zhang Y, Li J, Li Q, He Z. A modified micro reactor fueled with hydrogen for reducing entropy generation. Int J Hydrogen Energy 2019;44(51):27984–94. https://doi.org/10.1016/j.ijhydene.2019.09.009.

[21] Wang W, Zuo Z, Liu J, Yang W. Entropy generation analysis of fuel premixed CH4/H2/air flames using multistep kinetics. Int J Hydrogen Energy 2016;41(45):20744–52. https://doi.org/10.1016/j.ijhydene.2016.08.103.

[22] Datta A. Entropy generation in a confined laminar diffusion flame. Combust Sci Technol 2000;159:39–56. https://doi.org/10.1080/00102200008935776.

[23] Stanciu D, Isvoranu D, Marinescu M, Gogus Y. Second law analysis of diffusion flames. Int J Therm 2001;4(1):1–18.

[24] Datta A. Effects of gravity on structure and entropy generation of confined laminar diffusion flames. Int J Therm Sci 2005;44:429–40. https://doi.org/10.1016/j.ijthermalsci.2004.10.003.

[25] Chen S, Liu Z, Liu J, Li J, Wang L, Zheng C. Analysis of entropy generation in hydrogen-enriched ultra-lean counter-flow methane-air non-premixed combustion. Int J Hydrogen Energy 2010;35(22):12491–501. https://doi.org/10.1016/j.ijhydene.2010.08.048.

[26] Briones AM, Mukhopadhyay A, Aggarwal SK. Analysis of entropy generation in hydrogen-enriched methane-air propagating triple flames. Int J Hydrogen Energy 2009;34(2):1074–83. https://doi.org/10.1016/j.ijhydene.2008.09.103.

[27] Chen S, Han H, Liu Z, Li J, Zheng C. Analysis of entropy generation in non-premixed hydrogen versus heated air

counter-flow combustion. Int J Hydrogen Energy 2010;35:4736–46. https://doi.org/10.1016/j.ijhydene.2010.02.113.
[28] Raghavan V, Gogos G, Babu V, Sundararajan T. Entropy generation during the quasi-steady burning of spherical fuel particles. Int J Therm Sci 2007;46:589–604. https://doi.org/10.1016/j.ijthermalsci.2006.07.006.
[29] Pope DN, Raghavan V, Gogos G. Gas-phase entropy generation during transient methanol droplet combustion. Int J Therm Sci 2010;49:1288–302. https://doi.org/10.1016/j.ijthermalsci.2010.02.012.
[30] Farran R, Chakraborty N. A direct numerical simulation-based analysis of entropy generation in turbulent premixed flames. Entropy 2013;15(5):1540–66. https://doi.org/10.3390/e15051540.
[31] Ertesvåg IS, Kolbu J. Entropy Production modeling in CFD of turbulent combustion flow. In: Kjelstrup S, et al., editors. Proc. ECOS 2005 18th int. Conf. On efficiency, cost, optimization, simulation and environmental impact of energy systems, Trondheim 20-22 june 2005. Trondheim, Norway: Tapir Academic Press; 2005. p. 265–72.
[32] Emadi A, Emami MD. Analysis of entropy generation in a hydrogen-enriched turbulent non-premixed flame. Int J Hydrogen Energy 2013;38(14):5961–73. https://doi.org/10.1016/j.ijhydene.2013.02.115.
[33] Gholamalizadeh E, Alimoradi A, Saee AD, Amiri A, Moghaddam MG. Study of the heat transfer characteristics and entropy generation rate for the reacting flows inside tubes. Appl Therm Eng 2019;149:1435–44. https://doi.org/10.1016/j.applthermaleng.2018.12.119.
[34] Rajabi V, Amani E. A computational study of swirl number effects on entropy generation in gas turbine combustors. Heat Tran Eng 2019;40(3–4):346–61. https://doi.org/10.1080/01457632.2018.1429056.
[35] Marble F, Candel S. Acoustic disturbance from gas non-uniformities convected through a nozzle. J Sound Vib 1977;55(2):225–43. https://doi.org/10.1016/0022-460X(77)90596-X.
[36] Magri L, O'Brien J, Ihme M. Compositional inhomogeneities as a source of indirect combustion noise. J Fluid Mech 2016;799:R4. https://doi.org/10.1017/jfm.2016.397.
[37] Bazdidi-Tehrani F, Abedinejad MS, Mohammadi M. Analysis of relationship between entropy generation and soot formation in turbulent kerosene/air jet diffusion flames. Energy Fuels 2019;33(9):9184–95. https://doi.org/10.1021/acs.energyfuels.9b01671.
[38] Kooshkbaghi M, Frouzakis CE, Boulouchos K, Karlin IV. Entropy production analysis for mechanism reduction. Combust Flame 2014;161(6):1507–15. https://doi.org/10.1016/j.combustflame.2013.12.016.
[39] Porras S, Bykov V, Gol'dshtein V, Maas U. Joint characteristic timescales and entropy production analyses for model reduction of combustion systems. Entropy 2017;19(6):264. https://doi.org/10.3390/e19060264.
[40] Ream AE, Slattery JC, Cizmas PG. A method for generating reduced-order combustion mechanisms that satisfy the differential entropy inequality. Phys Fluids 2018;30(4):043601. https://doi.org/10.1063/1.5022691.
[41] Sadiki A, Hutter K. On thermodynamics of turbulence: development of first order closure models and critical evaluation of existing models. J. Non-Equil. Thermodyn. 2000;25:131–60. https://doi.org/10.1515/JNETDY.2000.009.
[42] Ahmadi G, Cao J, Schneider L, Sadiki A. A thermodynamical formulation for chemically active multiphase turbulent flows. Int J Eng Sci 2006;44:699–720. https://doi.org/10.1016/j.ijengsci.2006.06.001.
[43] Chen J, Choudhary A, de Supinski B, DeVries M, Hawkes E, Klasky S, Liao W, Ma K, Mellor-Crummey J, Podhorszki N, Sankaran R, Shende S, Yoo C. Terascale direct numerical simulations of turbulent combustion using S3D. Comput Sci Discov 2009;2(1):15001. https://doi.org/10.1088/1749-4699/2/1/015001.
[44] Haase R. Thermodynamics of irreversible processes. Reading, Massachusetts: Addison-Wesley; 1963.
[45] de Groot S, Mazur P. Non-equilibrium thermodynamics. New York: Dover Publications; 1984.
[46] Kee RJ, Dixon-Lewis G, Miller JA. A fortran computer code package for the evaluation of gas-phase multicomponent transport properties. SANDIA Rep. No. SAND86-8246, Sandia National Laboratories, Livermore, CA. 1986.
[47] Kee RJ, Dixon LG, Warnatz J, Coltrin ME, Miller JA, Moffat HK. A fortran chemical kinetics package for the analysis of gas-phase chemical kinetics. In: Tech. Rep., release 3.5. San Diego, CA: Reaction Design Inc.; 1999.
[48] Ertesvåg IS. Sensitivity of the chemical exergy for atmospheric gases and gaseous fuels to variation in ambient conditions. Energy Convers Manag 2007;48:1983–95. https://doi.org/10.1016/j.enconman.2007.01.005.
[49] Echekki T, Chen JH. Direct numerical simulation of autoignition in non-homogeneous hydrogen-air mixtures. Combust Flame 2003;134(3):169–91. https://doi.org/10.1016/S0010-2180(03)00088-9.
[50] Sankaran R, Hawkes ER, Chen JH, Lu TF, Law CK. Direct numerical simulations of turbulent lean premixed combustion. J. Phys. Conf. Series 2006;46(1):38–42. https://doi.org/10.1088/1742-6596/46/1/004.
[51] Gruber A, Sankaran R, Hawkes ER, Chen JH. Turbulent flame wall interaction: a direct numerical simulation study. J Fluid Mech 2010;658:5–32. https://doi.org/10.1017/S0022112010001278.
[52] Grout RW, Gruber A, Yoo CS, Chen JH. Direct numerical simulation of flame stabilization downstream of a traverse fuel jet in cross-flow. Proc Combust Inst 2011;33(1):1629–37. https://doi.org/10.1016/j.proci.2010.06.013.
[53] Hawkes ER, Sankaran R, Sutherland JC, Chen JH. Scalar mixing in DNS of temporally-evolving plane jet flames with detailed CO/H2 kinetics. Proc Combust Inst 2007;31(1):1633–40. https://doi.org/10.1016/j.proci.2006.08.079.
[54] Lignell DO, Chen JH, Smith PJ, Lu T, Law CK. The effect of flame structure on soot formation and transport in turbulent nonpremixed flames using direct numerical simulation. Combust Flame 2007;151(1–2):2–28. https://doi.org/10.1016/j.combustflame.2007.05.013.
[55] Kennedy CA, Carpenter MH. Several new numerical methods for compressible shear layer simulations. Appl Numer Math 1994;14(804):397. https://doi.org/10.1016/0168-9274(94)00004-2.
[56] Kee RJ, Rupley FM, Miller JA. CHEMKIN-II: a FORTRAN chemical kinetics package for the analysis of gas phase chemical kinetics. SANDIA Rep 1989:3–164. No. SAND89-8009B.
[57] Li J, Zhao Z, Kazakov A, Dryer FL. An updated comprehensive kinetic model of hydrogen combustion. Int J Chem Kinet 2004;36(10):566–75. https://doi.org/10.1002/kin.20026.
[58] Torabi M, Torabi M, Peterson GPB. Entropy generation of double diffusive forced convection in porous channels with thick walls and Soret effect. Entropy 2017;19(4):171. https://doi.org/10.3390/e19040171.